80065_Auto_Edited -Check.docx

Deep learning-based radiomics based on contrast-enhanced ultrasound predicts early recurrence and survival outcome in hepatocellular carcinoma

Huang Z et al. Deep learning-based radiomics predict

6 Abstract

BACKGROUND

Hepatocellular carcinoma (HCC) is the most common primary liver malignancy.

AIM

To predict early recurrence (ER) and overall survival (OS) in patients with HCC after radical resection using deep learning-based radiomics (DL radiomics).

METHODS

A total of 414 consecutive patients with HCC who underwent surgical resection with available preoperative grayscale and contrast-enhanced ultrasound images were enrolled. The clinical, DL radiomics, and clinical + DL radiomics model was then designed to predict ER and OS.

RESULTS

The DL radiomics model for predicting ER showed satisfactory clinical benefits (AUC 0.819, 0.568 in the training and testing cohorts), similar to clinical model (AUC 0.580, 0.520 in the training and testing cohorts, P > 0.05). The C-indices in predict of OS of the clinical + DL radiomics model in the training and testing cohorts were 0.800 and 0.759, respectively. The clinical + DL radiomics model and the DL radiomics model outperformed the clinical model in the training and testing cohorts (all P < 0.001). We divided patients into four categories by dichotomizing predicted ER and OS. Patients with class 1 (high ER rate and low risk of OS), retreatment (microwave ablation) after recurrence was associated with improved survival (HR 7.895, P = 0.005).

CONCLUSION

As compared to the clinical model, the clinical + DL radiomics model significantly improved the accuracy of predicting OS after radical resection of HCC.

Key Words: Hepatocellular carcinoma; Deep learning; Overall survival; Early recurrence; Contrast-enhanced ultrasound

Huang Z, Shu Z, Zhu RH, Xin JY, Wu LL, Wang HZ, Chen J, Zhang ZW, Luo HC, Li KY. Deep learning-based radiomics based on contrast-enhanced ultrasound predicts early recurrence and survival outcome in hepatocellular carcinoma. *World J Gastrointest Oncol* 2022; In press

Core Tip: Multivariate Cox regression analysis confirmed that age [hazard ratio (HR), 1.01], CA 19-9 (HR, 0.60), tumor size (HR, 1.11), echogenicity (HR, 0.82), and deep learning-based radiomics (HR, 4.33) were independent predictors of survival outcome (all P < 0.05). The concordance index of the clinical + deep learning-based radiomics model in the training and testing cohorts were 0.800 and 0.759, respectively. We divided patients into four categories by dichotomizing predicted early recurrence and survival outcome. We found that for patients with class 1 (high early recurrence rate and low risk of survival outcome), retreatment after recurrence was associated with improved survival.

INTRODUCTION

Hepatocellular carcinoma (HCC) is the most common primary liver malignancy^[1]. Surgical resection is considered the mainstream intervention for early HCC treatment^[2], and its therapeutic effect has gradually improved in recent years. However, the postoperative recurrence rate of HCC remains as high as 60% at the 5-¹¹ tar follow-up^[3], and the 5-year average survival rate is less than 32%^[4]. Previous studies have reported

that the prognosis of patients with early recurrence (ER) of HCC (within 1 year) after surgical resection is poorer than that of patients with late recurrence (> 1 year)^[5]. Therefore, to develop future treatment strategies, there is an urgent need to improve the identification of patients at high risk of recurrence and poor prognosis; this may help identify those who may benefit from adjuvant systemic therapy.

Clinical biomarkers, such as tumor burden, associated with postoperative recurrence and outcomes have been identified^[6]. However, the model based on these clinical biomarkers could not provide sufficient predictive power, and quantifiable measures and radiological information were not included in the model, which could provide essential information. Therefore, new representations of biomarker technology must be urgently explored to predict postoperative recurrence and patient outcomes more accurately.

Medical imaging is a potential method for HCC diagnosis^[7]. A previous study has developed a model that used clinical and contrast-enhanced computed tomography-based radiographic features to accurately predict the ER of HCC after surgical resection^[8]. Ultrasonography is widely used in HCC examination as it is cost-effective, widely available, and time-saving and provides real-time results. More importantly, contrast-enhanced ultrasonography (CEUS) can visualize the microcirculatory perfusion of HCC in real-time^[9]. The microbubble contrast agent can be safely used in patients with decreased renal function^[10].

Accurate prediction of early HCC recurrence and patient outcome is required to make clinical decisions before surgical resection. Traditional imaging features are relatively poor indicators of tumor heterogeneity (e.g., microvascular invasion and recurrence), are poor predictors of clinical outcomes^[11], and are highly subjective, difficult to quantify, and challenging to apply further. Radiomics analysis transforms raw images into countable quantitative features and interprets tumor pathophysiology^[12]. Neural network mining to link these features to biological and clinical endpoints can help develop models to predict patient outcomes, thereby improving prediction-based cancer management^[13]. Deep learning-based radiomics (DL

radiomics) has been applied to patients with HCC and has achieved promising results in predicting microvascular invasion and response to transarterial chemoembolization^[14,15].

This study aimed to predict ER and overall survival (OS) after radical resection of HCC by establishing a DL radiomics model using ultrasonographic and CEUS images.

MATERIALS AND METHODS

Patients

The institutional review boards of our institution approved this retrospective study and waived the requirement to obtain written informed consent of all participants.

We retrospectively screened 5466 patients with HCC meeting the Milan criteria who underwent curative resection of HCC at our institution between January 2008 and December 2018. HCC was diagnosed based on pathological findings^[16]. The exclusion criteria were as follows: (1) CEUS not performed; (2) recurrent lesions or a history of radiofrequency ablation, microwave ablation, or transcatheter arterial chemoembolization before CEUS; and (3) incomplete follow-up. A total of 5052 patients were excluded, leaving 414 in the final analysis (Supplementary Figure 1). Clinical features, including basic patient information, biological test results, and treatment-related information, were obtained from patient records.

CEUS has the following clinical indications: In patients at risk for HCC, ultrasound screening is positive for liver nodules according to current clinical practice standards, the World Federation for Ultrasound in Medicine and Biology (WFUMB)-European Federation of Societies for Ultrasound in Medicine and Biology (EFSUMB) and CEUS Liver Imaging Reporting and Data System (LI-RADS) guidelines; focal liver observation at single-phase CT or unenhanced MRI performed for other clinical reasons; indeterminate focal liver observation at multiphase contrast-enhanced CT or MRI; and definite HCC on CT or MRI images in reparation for or during tissue sampling, surgical resection, or percutaneous ablation treatment.

Ultrasonographic examination

CEUS was performed using a GE Logiq 9 scanner (GE Healthcare, Wauwatosa, WI, United States) with a 25-MHz frequency range transducer and a 3-5 L probe. Contrast agent (2.4 mL, SonoVue, Bracco, Milan, Italy) was injected intravenously, followed by flushing with 10 mL of 0.9% saline. Continuous observation of three-stage contrast enhancement was performed, including the arterial phase (0-30 s), portal phase (31-120 s), and late phase (121-360 s). CEUS inspections were recorded as video clips for analysis. For the CEUS image used for research, a frame of image with peak contrast intensity of the lesion is selected, that is, the frame of image with the maximum intensity is selected by quantitatively analyzing the enhanced intensity of the lesion in 0-360 s.

Two sonographers (one with more than 8 years of experience in CEUS and the other with more than 5 years of experience) who were blinded to the pathology results evaluated each lesion. In the event of a difference of opinion between the two readers, the final decision was made by a third blinded sonographer (with more than 20 years of CEUS experience). Tumor size, number, and satellite nodules on CEUS were evaluated. Nodules close to a primary tumor (< 3 cm) were designated as satellite nodules. During the late phase, the presence of perfusion defects surrounding HCC lesions was evaluated. If a nodule exhibited hypoechogenicity compared with the surrounding enhanced liver parenchyma, it was defined as the "presence of a perfusion defect of satellite nodules." The degree of enhancement of each lesion was compared with that of the surrounding normal liver tissue and classified as hyper-enhanced, iso-enhanced, or hypo-enhanced.

Follow-up protocol

The patients were followed up at 1, 3, 6, 9, and 12 mo after operation, and every 3-6 mo after 12 mo. At each follow-up, serum alpha-fetoprotein levels were measured and imaging (contrast-enhanced computed tomography, CEUS, or contrast-enhanced magnetic resonance imaging) was performed. ER was defined as intrahepatic and/or

extrahepatic recurrence of HCC within 1 year after resection. Given that an increasing serum alpha-fetoprotein level alone does not necessarily mean recurrence, recurrence was confirmed by radiological evidence of a new tumor. All patients were followed up until death, ER, or for at least 1 year after curative resection. OS was calculated as the time interval between the date of surgery and the date of death or last follow-up.

Construction and validation of model

Image quantification (radiomic feature extraction and deep learning-based radiomic feature extraction of grayscale image and CEUS image, which was a frame of image with peak contrast intensity of the lesion (Supplementary Figure 2), OS prognostic model construction and validation (including the development of deep learning-based radiomics score, OS prognostic model using clinical variables and DL radiomic score, and validation of prognostic models), and construction and validation of the model for ER prediction are shown in the supplementary material. We also assessed the ability of the DL radiomics model to improve the ability of three clinicians (with 11, 5, and 2 years of experience, respectively) to predict ER, with or without the assistance of the DL radiomics model. To demonstrate the impact of the DL radiomics model on clinician-individualized assessment performance, three clinicians independently reassessed each patient's ER status on the same day after accounting for the DL radiomics model predictions.

Statistical analysis

Differences in the distribution of clinical variables of the training and testing cohorts were assessed by Fisher's exact test or the chi-square test for categorical data and the nonparametric MannWhitney test for continuous data. To evaluate the predictive performance of the different model, we applied ROC curve and its AUC value. Accuracy, sensitivity, and specificity were calculated from the confusion matrix to quantitatively evaluate the predictive model. For prognostic models predicting ER, we used Kaplan-Meier analysis and the log-rank test to assess survival differences in

prognostic clinical variables and radiological characteristics between the training and test sets. Interclass correlation coefcients (ICC) were calculated for inter-observer and intra-observer agreement. A two-tailed P value less than 0.05 was considered as statistical significance. The whole statistical analysis and graphic production were completed by Python (version 3.8) and R (version 3.6.1).

RESULTS

Demographic characteristics

A total of 414 patients were included in this study, of which 289 and 125 were assigned to the training and testing cohorts, respectively. Mean age of 414 patients was 53 (45-60) years, 375 (90.6) male. The demographic characteristics of patients in the training and testing cohorts were compared (Table 1). There were no significant differences between the training and testing groups (P > 0.05). During a median follow-up period of 68 mo (range, 1-137 mo), 217 patients (52.4%) developed recurrence after curative surgical resection.

Prediction models for ER

We considered 414 grayscale ultrasonographic images and 414 peak contrast intensities of CEUS images. A total of 11270 radiological features were extracted from 414 patients. After univariate logistic regression selection, 898 features were retained. After the selection of the maximum relevance minimum redundancy, 8 features were selected as candidate features, and the preoperative prediction ER model was designed using L1-regularized logistic re-gression machine learning. Inter-observer ICC for measuring DL radiomics features ranged from 0.633 to 0.989. Intra-observer ICC for measuring DL radiomics features ranged from 0.689 to 0.927. The DL radiomics model had an AUC of 0.819 in the training cohort with 74% accuracy and an AUC of 0.568 in the test cohort with 58% accuracy.

In this study, the presence of satellites was selected to construct a clinical model based on the constants and satellites (Table 2). The clinical model had an AUC of 0.58 in

the training cohort with 56% accuracy and an AUC of 0.52 in the test cohort with 56% accuracy.

We constructed a clinical + DL radiomics model, including the presence of satellites and radiomic/DL features. The training cohort's AUC, accuracy, sensitivity, and specificity were 0.83, 73%, 71%, and 76%, respectively. The testing cohort's AUC, accuracy, sensitivity, and specificity were 0.57, 59%, 62%, and 56%, respectively. The DL radiomics model exhibited good classification performance based on ROC curves (Figure 1) and satisfactory clinical benefit (Figure 1), similar to those of the satellite lesion-based clinical model (P > 0.05). Prediction accuracy did not improve when clinical variables were combined with the DL radiomics model (AUC: 0.830 for the clinical + DL radiomics model in the training cohort; AUC: 0.572 for the clinical + DL radiomics model vs 0.568 for the DL radiomics model in the testing cohort).

In univariate FineGray regression analysis, satellite nodules, DL radiomics model, and multiple lesions were significantly associated with ER. Using these variables, we performed a multivariate FineGray competitive risk regression analysis. This analysis showed that the DL radiomics model remained a strong independent predictor of ER after adjusting for clinical variables (OR = 132.847, P < 0.001).

We found that human performance in predicting ER was significantly enhanced after integrating the DL radiomics model. For clinician 1, the sensitivity increased significantly from 0.250 to 0.856 in the training cohort and from 0.230 to 0.812 in the testing cohort. Likewise, for clinicians 2 and 3, the sensitivity of both testing cohorts increased significantly (0.248 to 0.855, 0.268 to 0.818 in the training cohort; 0.289 to 0.784, 0.307 to 0.823 in the testing cohort). Scores were consistent across clinicians with a κ value of 0.76-0.89 and were significantly improved by the integrated DL radiomics model, with a κ value of 0.93-0.97.

Prognostic model for OS

We obtained 11270 radiomics/DL features from patient images and selected them through univariate Cox proportional hazards regression, with 50 features with Harrell's concordance index (C-index) > 0.58. Multivariate Cox regression with L1 penalization calculates survival hazard values and builds high-risk and low-risk groups based on hazard values. The optimal stratification threshold for X-tile generation was 0.52. Kaplan-Meier curves showed significant differences between the low- and high-risk subgroups in the training and testing cohorts (Figure 2). Inter-observer ICC for measuring DL radiomics features ranged from 0.611 to 0.976. Intra-observer ICC for measuring DL radiomics features ranged from 0.699 to 0.912. The C-indices in the training and testing cohorts were 0.792 and 0.741, respectively. Calibration curves at 1, 3, or 5 years showed good agreement between DL radiomics model estimates and actual observations in the training and testing cohorts.

In univariate analysis, nine significant factors, including five clinical variables (age, sex, carcinoembryonic antigen, carbohydrate antigen 125, and carbohydrate antigen 19-9), three semantic imaging features (tumor size x, tumor size y, and unsmooth margins), and DL radiomics, were significantly associated with OS (both P <(Supplementary Table 1). Multivariate Cox regression analysis confirmed that age [hazard ratio (HR), 1.01; 95% confidence interval (CI), 1.00-1.03, P = 0.02], carbohydrate antigen 19-9 (HR, 0.6; 95%CI, 0.04-1.03, P = 0.007), tumor size y (HR, 1.11; 95%CI, 1.03-1.19, P = 0.001), and DL radiomics (HR, 4.33; 95%CI, 3.45-5.45, P < 0.005) were independent predictors of OS (Table 3). Based on the multivariate Cox regression analysis of assigned coefficients, these independent predictor variables were linearly combined to build a clinical and clinical + DL radiomics model. Kaplan-Meier curves showed significant differences between the low- and high-risk subgroups in the training and testing cohorts (Figure 2). The C-indices of the clinical model in the training and testing cohorts were 0.566 and 0.565, respectively. The C-indices of the clinical + DL radiomics model in the training and testing cohorts were 0.800 and 0.759, respectively. The clinical + DL radiomics model and DL radiomics model outperformed the clinical model in the training cohort ($\overline{P} < 0.001$ and P < 0.001, respectively). Similar results were observed in the testing cohort (P < 0.001, P < 0.001). The corresponding prediction error curves show that the prediction error of the clinical + DL radiomics model is consistently lower than that of the clinical model. Similar results were obtained for the combined Brier scores in the training and testing cohorts. Finally, we further quantified the improvement in survival prediction accuracy between the clinical + DL radiomics model and the clinical model. This resulted in a net reclassification improvement in survival of 0.234 (0.009 to 0.312; P < 0.001) and an OS net reclassification improvement of 0.176 (0.076 to 0.293; P < 0.001) in the testing cohort.

Histological features (degree of differentiation (HR, 1.76; 95%CI, 0.56-3.01, P = 0.012) and microvascular infiltration (HR, 2.25; 95%CI, 0.75-5.12, P = 0.023) were independent predictors of OS (Supplementary Table 2). The clinical + DL and DL radiomics models have the same performance with the histological features in the training cohort (P = 0.157 and P = 0.566, respectively). Similar results were observed in the testing cohort (P = 0.225 and P = 0.648, respectively).

Evaluation of model for predicting OS and benefit of retreatment after recurrence

In addition to evaluating the accuracy of the model in predicting ER and OS, we further evaluated the correlation between retreatment (microwave ablation) after recurrence and OS in patients. We divided patients into four categories by dichotomizing predicted ER and OS. We found that for patients with class 1 (high ER rate and low risk of OS), retreatment after recurrence was associated with improved survival (HR 7.895, P = 0.005). In contrast, for patients with class 2 (high ER rate and high risk of OS) (HR 1.542, P = 0.214), patients with class 3 (low ER rate and low risk of OS) (HR 0.357, P = 0.500), and patients with class 4 (low ER rate and high risk of OS) (HR 1.416, P = 0.234), retreatment after recurrence did not affect survival (Figure 3).

DISCUSSION

This study aimed to develop and validate a predictive model for ER and OS in patients with early-stage HCC undergoing surgical resection. This model allows for better

preoperative/pretreatment decision-making as to the best possible treatment options and timing. We transformed radiomics/DL signatures into quantitative radiomics/DL signatures and constructed a DL radiomics model with a better preoperative ability to predict patient OS than clinical models alone. This model may guide individualized treatment and survival monitoring.

Early-stage HCC still has a high recurrence rate after radical surgery. In our study, 52.4% of postoperative patients developed ER. Early HCC has high heterogeneity and an apparent prognosis, which should be determined early and accurately. Gene signatures have been widely used in tumor identification but are rarely used in clinical applications because of their high cost and time consumption. Considering the high recurrence rate of HCC after radical resection, including disseminated or recurrent disease, early prediction of ER is critical for improving individualized treatment. As a routine examination, ultrasonography has a high potential for further investigation of ER-predictive radiological features. With the development of machine learning technology, a large amount of quantitative radiological data has been used to construct more predictive models than those developed by semantic radiological features. Our study found that the DL radiomics score has the same or a higher ability to predict ER than satellite nodules. The DL radiomics score can predict the patient's ER before surgery, helping guide treatment choices.

In this study, we developed an ER-related DL radiomics model and evaluated its role in predicting OS. Furthermore, we combined clinical and DL radiomics features to predict OS. After the multivariate We found that age was a significant risk factor for OS in patients with HCC, consistent with the results of other studies^[8]. In addition, we found carbohydrate antigen 19-9, tumor size, and echogenicity were important risk factors for OS. However, the clinical + DL radiomics and DL radiomics models made a more dominant contribution in predicting OS than these clinical variables.

Re-surgical resection is considered a treatment for HCC recurrence. A key treatment issue is how to identify patients who may benefit from retreatment for HCC recurrence. However, given the costs associated with treatment, surgical trauma, and modest

survival benefits, the optimal criteria for selecting candidates for retreatment for HCC recurrence remain unclear. The model developed in this study can help identify such patients. By combining information on ER risk and survival, our model can identify patients with class 1 who are more likely to benefit from re-surgical resection treatment.

HCC is a tumor with a rich blood supply in which tortuous and dilated new vessels are continuously generated. In our study, the frame with the highest peak intensity in the arterial phase of CEUS was used, reflecting the density of neovascularization in the tumor. Studies have shown that the peak intensity in the recurrence group is lower than that in the non-recurrence group and that peak intensity is a risk factor for HCC recurrence^[17].

Liu *et al*^[18] analyzes CEUS images based on DL radiomics to predict progression-free survival of radiofrequency ablation and surgical resection and optimize radiofrequency ablation and surgical resection treatment options for patients with HCC. Our study is also based on DL radiomics analysis of CEUS images; the difference is that our study aims to predict the ER and OS of patients with HCC after surgical resection and provide guidance for retreatment after recurrence.

Our study has two significant limitations. First, this is a single-center study, and a multicenter prospective study with a larger patient population is needed to further validate the performance of our model. Second, regions of interest are segmented manually and have not been fully automated. Finally, washout is also an important aspect of the assessment of HCC, and other images of CEUS need to be fully studied in the future.

CONCLUSION

The DL radiomics model has the same satisfactory clinical benefit for predicting ER as the clinical model. Compared with the clinical model, the clinical + DL radiomics model and the DL radiomics model significantly improved the accuracy of predicting OS after radical resection of HCC.

6 ARTICLE HIGHLIGHTS

Research background

Hepatocellular carcinoma (HCC) is the most common primary liver malignancy.

Research motivation

To develop future treatment strategies, there is an urgent need to improve the identification of patients at high risk of recurrence and poor prognosis; this may help identify those who may benefit from adjuvant systemic therapy.

Research objectives

To predict early recurrence (ER) and overall survival (OS) in patients with HCC after radical resection using deep learning-based radiomics (DL radiomics).

Research methods

A total of 414 consecutive patients with HCC who underwent surgical resection with available preoperative grayscale and contrast-enhanced ultrasound images were enrolled. The clinical, deep learning (DL) radiomics, and clinical + DL radiomics model was then designed to predict ER and OS.

Research results

The DL radiomics model for predicting ER showed satisfactory clinical benefits (AUC 0.819, 0.568 in the training and testing cohorts), similar to clinical model (AUC 0.580, 0.520 in the training and testing cohorts, P > 0.05). The C-indices in predict of OS of the clinical + DL radiomics model in the training and testing cohorts were 0.800 and 0.759, respectively. The clinical + DL radiomics model and the DL radiomics model outperformed the clinical model in the training and testing cohorts (all P < 0.001). We divided patients into four categories by dichotomizing predicted ER and OS. Patients with class 1 (high ER rate and low risk of OS), retreatment (microwave ablation) after recurrence was associated with improved survival (HR 7.895, P = 0.005).

Research conclusions

As compared to the clinical model, the clinical + DL radiomics model significantly improved the accuracy of predicting OS after radical resection of HCC.

Research perspectives

As compared to the clinical model, the clinical + DL radiomics model significantly improved the accuracy of predicting OS after radical resection of HCC.

Figure Legends

Receiver operating characteristic curves and decision curve analysis. A:
Receiver operating characteristic curves of clinical, deep learning-based radiomics (DLR), and clinical + DLR models for predicting early recurrence in the training and testing cohorts; B: Decision curve analysis (DCA) of each model in predicting early recurrence. The vertical axis measures standardized net benefit. The horizontal axis shows the corresponding risk threshold. The DCA showed that if the threshold probability is between 0 and 1, using the DL radiomics model derived in the present study to predict ER provided as same benefit as clinical model. ROC: Receiver operating characteristic; DCA: Decision curve analysis; DLR: Deep learning-based radiomics.

Figure 2 Kaplan-Meier curves of overall survival stratified by high and low risk for clinical, deep learning-based radiomics, and clinical + deep learning-based radiomics models. A and B: Clinical training; C and D: Deep learning-based radiomics (DLR) testing; E and F: Clinical + deep learning-based radiomics training. DLR: Deep learning-based radiomics.

Figure 3 Relationship between the deep learning-based radiomics model and benefit from retreatment after recurrence in matched patients. A: Four different risk classes were defined by early recurrence and overall survival predicted by the deep learning-based radiomics model; B: Kaplan-Meier curves of disease-free survival for patients who are stratified according to receipt of retreatment after recurrence.

Table 1 Patient characteristice

	Study	Training cohort	Testing	P value
	Population (n	(n = 289)	cohort (n =	
	= 414)		125)	
Age	53.00 (45.00-	52.059 ± 12.190	53.216 ±	0.1988
	60.00)		11.380	
Gender, n (%)				
Male	375 (90.6)	262 (90.7)	113 (90.4)	0.9196
BMI, kg/m ²	24.50 ± 4.20	24.10 ± 3.20	24.70 ± 3.40	0.1889
HBsAg-positive, n (%)	375 (90.6)	264 (91.3)	111 (88.8)	0.5274
AFP > 7 ng/mL, n (%)	292 (70.5)	205 (70.9)	87 (69.6)	0.8761
CEA > 5 ng/ml, n (%)	31 (7.5)	24 (8.3)	7 (5.6)	0.4494
CA125 > 40 ng/mL, <i>n</i>	15 (3.6)	8 (2.8)	7 (5.6)	0.2588
(%)				
CA199 > 34 ng/mL, n	46 (11.1)	295 (10.0)	17 (13.6)	0.3738
(%)				
WBC count, $/\mu L$	6262 ± 1985	6232 ± 1756	6354 ± 2125	0.5668
ALT, U/L	49 ± 36	48 ± 39	51 ± 41	0.1654
AST, U/L	51 ± 35	49 ± 36	53 ± 42	0.2358
Liver cirrhosis, n (%)	345 (83.3)	244 (84.4)	101 (80.8)	0.3630
Microvascular invasion,	312 (75.4)	211 (73.0)	101 (80.8)	0.0910
n (%)				
Tumor size, cm				
x	2.40 [1.70-3.68]	2.957 ± 1.850	3.120 ± 2.050	0.3689
y	2.00 [1.42-3.10]	2.480 ± 1.490	2.670 ± 1.960	0.4820
Gray-scale echogenicity				0.5954
Hyperechoic	46 (11.1)	35 (12.1)	11 (8.8)	
Medium	4 (1.0)	3 (1.0)	1 (0.8)	
Hypoechoic	364 (87.9)	251 (86.9)	113 (90.4)	

Arterial phase					0.4639
Hyperenhancemet		403 (97.3)	283 (97.9)	120 (96.0)	
Isoenhancement		8 (1.9)	4 (1.4)	4 (3.2)	
Hypoenhancement		3 (0.7)	2 (0.7)	1 (0.8)	
Portal phase					0.6669
Hyperenhancemet		15 (3.5)	12 (4.2)	3 (2.4)	
Isoenhancement		232 (56.0)	162 (56.1)	70 (56.0)	
Hypoenhancement		167 (40.3)	115 (39.8)	52 (41.6)	
Late phase					0.1300
Hyperenhancemet		2 (0.5)	1 (0.3)	1 (0.8)	
Isoenhancement		79 (19.1)	46 (15.9)	33 (90.4)	
Hypoenhancement		333 (80.4)	232 (80.3)	101 (80.8)	
Enhancing Caspsule		45 (10.9)	36 (12.5)	9 (7.2)	0.1598
Unsmooth Margins		97 (23.4)	64 (22.19)	33 (26.4)	0.4168
Retreatment	after	168 (40.3)	118 (40.5)	50 (40.0)	0.9270
recurrence					

BMI: Body mass index; AFP: Alphafetoprotein; CEA: Carcinoembryonic antigen; CA125: Carbohydrate antigen 125; CA199: Carbohydrate antigen 199; BCLC: Barcelona-clinic liver cancer; WBC: White blood cell; ALT: Alanine aminotransferase; AST: Aspartate aminotransferase.

Table 2 Univariate and multivariable analysis of the early recurrence of hepatocellular carcinoma patients

Univariate cox regression			Multivariate			ogistic	
				regressi	on		
HR	[0.025	0.975]	P	HR	[0.025	0.975]	P
0.991	0.971	1.011	0.383				
1.005	0.463	2.181	0.990				
1.138	0.472	2.740	0.773				
0.622	0.361	1.071	0.087	0.709	0.406	1.239	0.227
0.944	0.352	2.535	0.910				
1.811	0.424	7.752	0.423				
1.636	0.727	3.684	0.234				
1.248	<mark>0</mark> .697	2.321	<mark>0</mark> .267				
1 .566	0.397	2.108	<mark>0</mark> .675				
1.212	0.431	1.986	0.742				
1.142	0.506	2.121	0.657				
1.000	0.882	1.143	0.951				
0.988	0.856	1.142	0.873				
0.731	0.493	1.087	0.121				
0.924	0.351	2.438	0.874				
1.321	0.832	2.100	0.238				
0.982	0.512	1.885	0.957				
0.930	0.413	2.096	0.862				
	0.991 1.005 1.138 0.622 0.944 1.811 1.636 1.248 1.566 1.212 1.142 1.000 0.988 0.731	0.991 0.971 1.005 0.463 1.138 0.472 0.622 0.361 0.944 0.352 1.811 0.424 1.636 0.727 1.248 0.697 1.566 0.397 1.212 0.431 1.142 0.506 1.000 0.882 0.988 0.856 0.731 0.493 0.924 0.351 1.321 0.832 0.982 0.512	0.991 0.971 1.011 1.005 0.463 2.181 1.138 0.472 2.740 0.622 0.361 1.071 0.944 0.352 2.535 1.811 0.424 7.752 1.636 0.727 3.684 1.248 0.697 2.321 1.566 0.397 2.108 1.212 0.431 1.986 1.142 0.506 2.121 1.000 0.882 1.143 0.988 0.856 1.142 0.731 0.493 1.087 0.924 0.351 2.438 1.321 0.832 2.100 0.982 0.512 1.885	0.991 0.971 1.011 0.383 1.005 0.463 2.181 0.990 1.138 0.472 2.740 0.773 0.622 0.361 1.071 0.087 0.944 0.352 2.535 0.910 1.811 0.424 7.752 0.423 1.636 0.727 3.684 0.234 1.248 0.697 2.321 0.267 1.566 0.397 2.108 0.675 1.212 0.431 1.986 0.742 1.142 0.506 2.121 0.657 1.000 0.882 1.143 0.951 0.988 0.856 1.142 0.873 0.731 0.493 1.087 0.121 0.924 0.351 2.438 0.874 1.321 0.832 2.100 0.238 0.982 0.512 1.885 0.957	HR [0.025 0.975] P HR 0.991 0.971 1.011 0.383 1.005 0.463 2.181 0.990 1.138 0.472 2.740 0.773 0.622 0.361 1.071 0.087 0.709 0.944 0.352 2.535 0.910 1.811 0.424 7.752 0.423 1.636 0.727 3.684 0.234 1.248 0.697 2.321 0.267 1.566 0.397 2.108 0.675 1.212 0.431 1.986 0.742 1.142 0.506 2.121 0.657 1.000 0.882 1.143 0.951 0.988 0.856 1.142 0.873 0.731 0.493 1.087 0.121 0.924 0.351 2.438 0.874 1.321 0.832 2.100 0.238 0.982 0.512 1.885 0.957	0.991 0.971 1.011 0.383 1.005 0.463 2.181 0.990 1.138 0.472 2.740 0.773 0.622 0.361 1.071 0.087 0.709 0.406 0.944 0.352 2.535 0.910 1.811 0.424 7.752 0.423 1.636 0.727 3.684 0.234 1.248 0.697 2.321 0.267 1.566 0.397 2.108 0.675 1.212 0.431 1.986 0.742 1.142 0.506 2.121 0.657 1.000 0.882 1.143 0.951 0.988 0.856 1.142 0.873 0.731 0.493 1.087 0.121 0.924 0.351 2.438 0.874 1.321 0.832 2.100 0.238 0.982 0.512 1.885 0.957	HR [0.025 0.975] P HR [0.025 0.975] 0.991 0.971 1.011 0.383 0.463 2.181 0.990 0.463 2.181 0.990 0.406 1.239 0.622 0.361 1.071 0.087 0.709 0.406 1.239 0.944 0.352 2.535 0.910 0.423 0.423 0.423 0.424 7.752 0.423 0.267 0.267 0.267 0.267 0.267 0.267 0.675 0.675 0.675 0.675 0.657 0.657 0.657 0.657 0.657 0.657 0.657 0.0882 1.143 0.951 0.0873 0.0731 0.493 1.087 0.121 0.0924 0.351 2.438 0.874 0.874 0.924 0.351 2.438 0.874 0.957 0.982 0.512 1.885 0.957 0.957 0.957 0.957 0.957 0.957 0.957 0.957 0.957 0.957 0.957 0.975

capsules Satellite 4.843 1.917 12.244 0.001 4.194 1.368 12.871 0.012 nodules Umsmooth 0.839 0.4621.522 0.563 margins 0.990 0.707 0.953 Constant 1.387 FIB-4 score = Age (years) × AST (U/L) / $\sqrt{\text{platelet count} (10^9/L) \times \text{ALT (U/L)}}$. AFP: Alphafetoprotein; CEA: Carcinoembryonic antigen; CA125: Carbohydrate antigen125; CA199: Carbohydrate antigen199; ALT: Alanine aminotransferase; AST: Aspartate Fibrosis-4 aminotransferase; FIB-4 score: score.

Table 3 Univariate and multivariable analysis of the overall survival of hepatocellular carcinoma patients

		Univariate cox regression			Mult	Multivariate			
						regre	ession		
		HR	[0.025	0.975]	P	HR	[0.025	0.975]	P
Age		1.020	1.000	1.030	0.010	1.02	1.00	1.03	0.01
Gender		1.570	1.030	2.390	0.030	1.42	0.89	2.26	0.14
HBsAg-positiv	re	1.600	1.030	2.490	0.040	1.32	0.82	2.12	0.25
AFP		1.100	0.830	1.460	0.500				
CEA		0.760	0.460	1.270	0.300				
CA125		0.580	0.280	1.220	0.150				
CA199		0.630	0.420	0.950	0.030	0.65	0.41	1.03	0.07
ALT, U/L		1 .121	0.453	1.976	0.430				
AST, U/L		1.342	<mark>0</mark> .876	2.014	<mark>0</mark> .540				
FIB-4 Score		1.012	0.547	1.743	0.720				
Liver cirrhosis		1.112	0.563	1.956	0.550				
Tumor size x		1.080	1.010	1.160	0.040	0.96	0.85	1.09	0.56
Tumor size y		1.090	1.020	1.170	0.010	1.17	1.02	1.33	0.02
Gray-scale		0.830	0.670	1.020	0.080	0.77	0.60	0.99	0.04
echogenicity									
Arterial	phase	0.680	0.420	1.110	0.130				
enhancement									
Portal	phase	1.270	0.990	1.620	0.060	1.25	0.95	1.63	0.11
enhancement									
Portal	phase	1.130	0.810	1.580	0.460				
Enhancement									
Enhancing cap	sules	1.110	0.720	1.710	0.630				
Satellite nodul	es	1.190	0.780	1.830	0.420				
Unsmooth ma	rgins	0.720	0.520	0.990	0.040	0.79	0.56	1.13	0.19

Early reoccurence	ce	1.290	0.990	1.680	0.060	1.25	0.93	1.67	0.14
Retreatment	after	0.710	0.540	1.160	0.300				
recurrence									
DL radiomics		3.240	2.670	3.930	< 0.005				

AFP: Alphafetoprotein; CEA: Carcinoembryonic antigen; CA125: Carbohydrate antigen125; CA199: Carbohydrate antigen199; ALT: Alanine aminotransferase; AST: Aspartate aminotransferase; FIB-4 score: Fibrosis-4 score.

80065_Auto_Edited -Check.docx

ORIGINALITY REPORT

32%

SIMILARITY INDEX

PRIMARY SOURCES

- Yuming Jiang, Zhicheng Zhang, Qingyu Yuan, Wei Wang et al. "Predicting peritoneal recurrence and disease-free survival from CT images in gastric cancer with multitask deep learning: a retrospective study", The Lancet Digital Health, 2022 Crossref
- $\begin{array}{c} \text{link.springer.com} \\ \text{Internet} \end{array} \hspace{0.2in} 185 \text{ words} 3\%$
- Yuhan Yang, Yin Zhou, Chen Zhou, Xuelei Ma. "Deep 152 words 3% learning radiomics based on contrast enhanced computed tomography predicts microvascular invasion and survival outcome in early stage hepatocellular carcinoma", European Journal of Surgical Oncology, 2021
- www.karger.com
 Internet

 80 words 1 %
- Hui Zhang, Fanding Huo. "Prediction of early recurrence of HCC after hepatectomy by contrastenhanced ultrasound-based deep learning radiomics", Frontiers in Oncology, 2022

 Crossref
 - www.wjgnet.com
 Internet

 70 words 1 %

7	pubs.rsna.org Internet	61 words — 1 %
8	www.science.gov Internet	57 words — 1 %
9	ojrd.biomedcentral.com Internet	44 words — 1 %
10	"ECR 2019: Book of Abstracts", Insights into Imaging, 2019 Crossref	39 words — 1 %
11	bsdwebstorage.blob.core.windows.net	39 words — 1 %
12	2017.wco-iof-esceo.org	34 words — 1 %
13	www.researchsquare.com Internet	33 words — 1 %
14	Yuxue Xie, Yibo Dan, Hongyue Tao, Chenglong Wang, Chengxiu Zhang, Yida Wang, Jiayu Yang, Guang Yang, Shuang Chen. "Radiomics Feature Analysis of Cartilag Subchondral Bone in Differentiating Knees Predispose Posttraumatic Osteoarthritis after Anterior Cruciate I	ge and ed to
	Reconstruction from Healthy Knees", BioMed Resear International, 2021 Crossref	ch
15	International, 2021	32 words — 1 %

Patients With Soft Tissue Sarcoma ", Journal of Magnetic Resonance Imaging, 2022

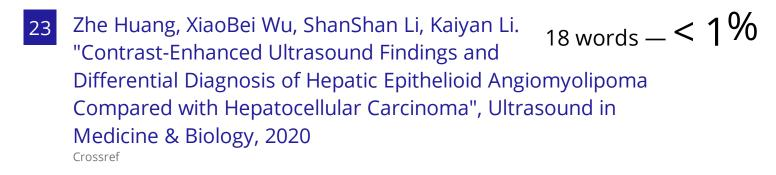
Crossref

- "American Transplant Congress 2007 Executive and Program Planning Committees and Abstract Review Committees", American Journal of Transplantation, 5/2007
- Xu Yang, Jun Liu, Xia Lu, Ying Kan, Wei Wang, Shuxin Zhang, Lei Liu, Hui Zhang, Jixia Li, Jigang Yang. "Development and Validation of a Nomogram Based on 18F-FDG PET/CT Radiomics to Predict the Overall Survival in Adult Hemophagocytic Lymphohistiocytosis", Frontiers in Medicine, 2021

 Crossref
- www.mdpi.com
 Internet 23 words < 1 %
 - Zaya Duisyenbi, Kazushi Numata, Hiromi
 Nihonmatsu, Hiroyuki Fukuda et al. "Comparison
 Between Low Mechanical Index and High Mechanical Index
 Contrast Modes of Contrast-Enhanced Ultrasonography:
 Evaluation of Perfusion Defects of Hypervascular Hepatocellular
 Carcinomas During the Post-Vascular Phase", Journal of
 Ultrasound in Medicine, 2019

Crossref

- 21 www.nature.com 21 words < 1 %
- Qin Xiachuan, Zhou xiang, Liu xuebing, Luo yan. "Predictive Value of Contrast-enhanced Ultrasound for Early Recurrence of Single Lesion Hepatocellular Carcinoma After Curative Resection", Ultrasonic Imaging, 2018 Crossref



www.frontiersin.org 18 words — < 1 %

www.ncbi.nlm.nih.gov

Qiao Ji, Guihua Liu, Xiangzhou Sun, Guangjian Liu, $_{16 \text{ words}} - < 1\%$ Mingde Lu, Xiaoyan Xie, Ming Xu, Yuanyuan Zhang, Shuguang Zheng. "Liver specific phase of perflubutane microbubbles contrast-enhanced ultrasound for potential use in the diagnosis of focal liver lesions", Journal of X-Ray Science and Technology, 2013

Crossref

- $_{\text{Internet}}^{\text{27}}$ jkms.org $_{\text{Internet}}^{\text{28}}$ 16 words -<1%
- www.sochob.cl 16 words < 1 %
- moam.info $_{\text{Internet}}$ 15 words -<1%
- Shen Li, Yadi Li, Min Zhao, Pengyuan Wang, Jun Xin. "Combination of F-Fluorodeoxyglucose PET/CT Radiomics and Clinical Features for Predicting Epidermal Growth Factor Receptor Mutations in Lung Adenocarcinoma ", Korean Journal of Radiology, 2022 Crossref

31	assets.researchsquare.com
J 1	Internet

- $_{14 \, \text{words}} = < 1\%$
- "ECR 2018 BOOK OF ABSTRACTS", Insights into Imaging, 2018

 Crossref

 13 words -<1%
- Meike Dirks, Kim Haag, Henning Pflugrad, Anita B. $_{12\,\text{words}} < 1\%$ Tryc et al. "Neuropsychiatric symptoms in hepatitis C patients resemble those of patients with autoimmune liver disease but are different from those in hepatitis B patients", Journal of Viral Hepatitis, 2019 $_{\text{Crossref}}$
- S. Li, L. Zhou, R. Chen, Y. Chen, Z. Niu, L. Qian, Y. Fang, L. Xu, H. Xu, L. Zhang. "Diagnostic efficacy of contrast-enhanced ultrasound versus MRI Liver Imaging Reporting and Data System (LI-RADS) for categorising hepatic observations in patients at risk of hepatocellular carcinoma", Clinical Radiology, 2020
- Zeju Li, Yuanyuan Wang, Jinhua Yu, Yi Guo, Wei Cao. "Deep Learning based Radiomics (DLR) and its usage in noninvasive IDH1 prediction for low grade glioma", Scientific Reports, 2017

 Crossref
- tessera.spandidos-publications.com 12 words < 1%
- www.openaccessjournals.com 12 words < 1%
- Tomonari Shimagaki, Tomoharu Yoshizumi, Shinji 11 words <1% ltoh, Norifumi Iseda et al. "The ratio of serum des gamma carboxy prothrombin to tumor volume as a new

biomarker for early recurrence of resected hepatocellular carcinoma", Hepatology Research, 2022

Crossref

39	bmcgastroenterol.biomedcentral.com Internet	11 words $-<1\%$
40	pdfs.semanticscholar.org	10 words — < 1 %

- Jianxing Zeng, Jinhua Zeng, Kongying Lin, Haitao Lin, Qionglan Wu, Pengfei Guo, Weiping Zhou, Jingfeng Liu. "Development of a machine learning model to predict early recurrence for hepatocellular carcinoma after curative resection", Hepatobiliary Surgery and Nutrition, 2021 $^{\text{Crossref}}$
- Shan Jiang, Zhaolei Cui, Jianfeng Zheng, Qiaoling $_{9 \text{ words}} < 1\%$ Wu, Haijuan Yu, Yiqing You, Chaoqiang Zheng, Yang Sun. "Significance of immunogenic cell death-related prognostic gene signature in cervical cancer prognosis and antitumor immunity", Research Square Platform LLC, 2022 Crossref Posted Content

43 wjso.biomedcentral.cor	9 words — < 1 %
44 www.ghrnet.org	9 words — < 1 %
45 www.ighg.org	9 words — < 1 %

Guido Menozzi, Valeria Maccabruni, Ermanno
Gabbi, Giacomo Magnani, Elisa Garlassi.

8 words — < 1%

"Evaluation with contrast ultrasound of the prevalence of

splenic infarction in left-sided infective endocarditis", Journal of Ultrasound, 2014

Crossref

- Hui Huang, Si-min Ruan, Meng-fei Xian, Ming-de Li et al. "Contrast-enhanced ultrasound-based ultrasomics score: a potential biomarker for predicting early recurrence of hepatocellular carcinoma after resection or ablation", The British Journal of Radiology, 2021 $_{\text{Crossref}}$
- Seong Hyun Kim, Hyo K. Lim, Won Jae Lee, Dongil Choi, Cheol Keun Park. "Scirrhous hepatocellular carcinoma: Comparison with usual hepatocellular carcinoma based on CT–pathologic features and long-term results after curative resection", European Journal of Radiology, 2009
- Shihui Wang, Yi Wei, Zhouli Li, Jingya Xu, Yunfeng Zhou. "Development and Validation of an MRI Radiomics-Based Signature to Predict Histological Grade in Patients with Invasive Breast Cancer", Breast Cancer: Targets and Therapy, 2022 Crossref
- Wang, Yingqiang, Qianqian Luo, Youping Li, Shaolin $_{8\,\text{words}} < 1\%$ Deng, Shiyou Wei, and Xianglian Li. "Radiofrequency Ablation versus Hepatic Resection for Small Hepatocellular Carcinomas: A Meta-Analysis of Randomized and Nonrandomized Controlled Trials", PLoS ONE, 2014.
- Xujie Gao, Tingting Ma, Jingli Cui, Yuwei Zhang, Lingwei Wang, Hui Li, Zhaoxiang Ye. "A CT-based Radiomics Model for Prediction of Lymph Node Metastasis in Early Stage Gastric Cancer", Academic Radiology, 2020 Crossref

52	cjcr.amegroups.com Internet	8 words — <	1%
53	cyberleninka.org	8 words — <	1%
54	mdanderson.influuent.utsystem.edu Internet	8 words — <	1%
55	www.ilca2020.org	8 words — <	1%
56	www.nice.org.uk Internet	8 words — <	1%
57	www.thno.org Internet	8 words — <	1%
58	Yanghua Fan, Panpan Liu, Yiping Li, Feng Liu, Yu He, Liang Wang, Junting Zhang, Zhen Wu. "Non-Invasive Preoperative Imaging Differential Diagnos Intracranial Hemangiopericytoma and Angiomatou Meningioma: A Novel Developed and Validated Mc MRI-Based Clini-Radiomic Model", Frontiers in Oncorressive	ıs ultiparametric	1%
59	"APASL Seoul 2008 Meeting", Hepatology International, 2008 Crossref	6 words — <	1%
60	"Myocardial Ischemia and Infarction", Journal of the American College of Cardiology, 20060221 Crossref	6 words — <	1%
61	Hai-Bin Tu, Li-Hong Chen, Yu-Jie Huang, Si-Yi Feng, Jian-Ling Lin, Yong-Yi Zeng, "Novel model	6 words — <	1%

Jian-Ling Lin, Yong-Yi Zeng. "Novel model

combining contrast-enhanced ultrasound with serology

predicts hepatocellular carcinoma recurrence after hepatectomy", World Journal of Clinical Cases, 2021

Crossref

EXCLUDE QUOTES OFF EXCLUDE SOURCES OFF
EXCLUDE BIBLIOGRAPHY OFF EXCLUDE MATCHES OFF